applied sciences

MDPI

Article

Ab-Initio Investigations on Hydrogen Dissociation and Cross-Linking of Hydrocarbon Chains of Self-Assembled Monolayers of Alkanes

Yan Zhu [1], Xin-Yuan Wei [2] and Run Xu [3,*]

[1] Shanghai Technical Institute of Electronics & Information, Shanghai 201411, China; zhuyan@kust.edu.cn
[2] State Key Laboratory of Surface Physics, Department of Physics, Fudan University, Shanghai 200433, China; xinyuanwei@fudan.edu.cn
[3] School of Materials Science and Engineering, Shanghai University, Shanghai 200444, China
* Correspondence: runxu@shu.edu.cn; Tel.: +86-335-309-602

Abstract: First-principles calculations were carried out to study the structural and electronic properties of hydrocarbon chains of self-assembled monolayers with hydrogen dissociation. It was found that the incoming hydrogen could lead to the formation of H_2 molecules by stripping the nearby hydrogen atoms in the chains and thereby leave the neighboring carbon atoms to be free radicals. Two parallel hydrocarbon chains with dangling bonds can form a direct C-C bond, i.e., cross-linking happens between the two chains, which is ascribed to a charge accumulation in the cross-linking region. The polymerization of short molecules into long hydrocarbon chains through a different cross-linking mode is also discussed.

Keywords: self-assembled monolayers; alkane; cross-linking; hydrogen dissociation; first-principles calculation

check for updates

Citation: Zhu, Y.; Wei, X.-Y.; Xu, R. Ab-Initio Investigations on Hydrogen Dissociation and Cross-Linking of Hydrocarbon Chains of Self-Assembled Monolayers of Alkanes. *Appl. Sci.* **2022**, *12*, 6020. https://doi.org/10.3390/app12126020

Academic Editor: Cezary Czaplewski

Received: 22 April 2022
Accepted: 10 June 2022
Published: 14 June 2022

1. Introduction

Alkanes and other simple molecules based on carbon-hydrogen bonds are the building blocks of complex organic molecules and materials. Functionalization of C-H bonds in these kinds of materials are of great significance for environmental sustainability and economic development [1–4]. Besides, ultrathin organic films have been studied extensively due to their potential applications in materials science. For instance, they could be used as organic microelectronic and optoelectronic devices [5–7]. To carry out the applications, the technique of cross-linking between carbon atoms in different organic molecules is crucial [8–11]. Take Liu et al.'s work as an example, it shows the evidence for cross-links formed between the long-chain molecules on dotriacontane ($C_{32}H_{66}$) thin film [12]. The cross-linking of organic materials can be realized through various methods. The most common method is through using chemical additives or catalysts, the so-called wet procedure [13–17]. However, this procedure may be harmful to microelectronic devices because the chemical additives or catalysts may dramatically change the dielectric constant and other electronic properties, and hence the electronic transport of the devices. To avoid these disadvantages, a more physical method, a so-called dry procedure, was proposed to realize the cross-linking, which is based on collision-induced hydrogen dissociation by using electron beam or other charged particle beam bombardments [18–23]. This method, however, still has some drawbacks, such as the defects induced by the electrons damaging the original structure. The high energy cost is also a challenge for the charged particle accelerator or control instrument. These factors restrict the application range of this method. Therefore, a suitable method to realize the cross-linking of organic materials should have following characters: (1) avoiding introducing extra dopants or elements; (2) selectively dissociating the C-H bonds, without impact on C-C or other bonds; (3) low system complexity and energy-cost, suitable for large-scale industrial applications. The research of

Zhang et al. showed that a low-energy proton beam could be used to bombard the organic thin film and realize the cross-linking of organic molecules by selectively cleaving C-H bonds while keep other bonds unaffected [24–26]. As the proton is a positive charged particle, its application is restricted owing to the electronic insulating behavior of most organic materials. For these materials, a surface charging problem, i.e., the accumulated charge on the surface, will cause the irreversible change in the properties of the organic materials. Trebicky et al. proposed that H_2 molecules could be used as the incident particles to make the cross-linking [27]. The employment of neutral particle beams provides a new perspective for the fabrication of ultrathin organic films. However, systematic investigations of the role of H or H_2 played in this procedure are limited so far.

In this article, we investigate the structural and electronic properties of hydrocarbon chains with hydrogen collision [28]. The results are compared with the cases of the incidence of H_2 molecules. To the best of our knowledge, no such research has been reported from ab-initio calculations up to now. In this research, we chose the alkane-type hydrocarbon chain as the organic material because alkanes are a common polymer precursor and widely used as a functional organic material by appending appropriate functional groups [29,30]. Furthermore, the structure of an alkane is quite simple (C_nH_{2n+2}). Here, we first study the structural and electronic properties of infinitely long hydrocarbon chains with hydrogen dissociations. The cross-linking of two adjacent hydrocarbon chains was then explored and discussed. The case of $C_{20}H_{42}$, a finitely long molecule, was further investigated to see what happens.

2. Materials and Methods

The calculations were performed based on density functional theory (DFT) with exchange-correlation interaction described by the projector-augmented wave method (PAW) [31,32] in generalized gradient approximations (GGA) [33] with PW91 form [34], implemented in VASP software [35]. The employed cut-off energy of the plane waves was 500 eV. The convergent criterion of total energy was set as 10^{-5} eV per supercell. The force convergence criterion was smaller than 0.02 eV/Å. For all calculations, Monkhorst–Pack k-point sampling grids of $8 \times 8 \times 2$ were used [36]. The supercell (seen Figure 1a) contained 20 carbon and 40 hydrogen atoms with a length of 25.38 Å in the *z* direction [37]. The lattice constants of the supercell in the *x* and *y* axes were set to be a = b = 20 Å, which was large enough to minimize the unwanted interactions between the adjacent chains. Three initial adsorption sites were considered, labeled as s1, s2, and s3, as shown in Figure 1a. For site s1, the H atom was located in the plane perpendicular to the *z*-axis of the hydrocarbon chain. For site s2, the H atom was in the same plane but above the middle point of the C-H bond (bridge site). While for site s3, the adsorbed H atom was in one of the hydrogen columns along the *z*-axis. All these sites represent the configurations for the possible transition site. The initial distance from the H atom to the nearest hydrogen atom in the hydrocarbon chain for all the three cases was set to be 0.74 Å, i.e., the typical bond length of a H_2 molecule. The positions of the atoms were fixed for the calculations of the three initial configurations.

The stability of the three typical adsorption sites for H and H_2 were explored by the calculations of the adsorption energy, defined as:

$$E_a = E_{hc+adatom} - E_{hc} - E_{adatom} \quad (1)$$

where $E_{hc+adatom}$ is the total energy of a hydrocarbon chain with one H or H_2 adsorbed in the supercell. E_{hc} and E_{adatom} are the corresponding total energies of the hydrocarbon chain and an isolated H or H_2, respectively.

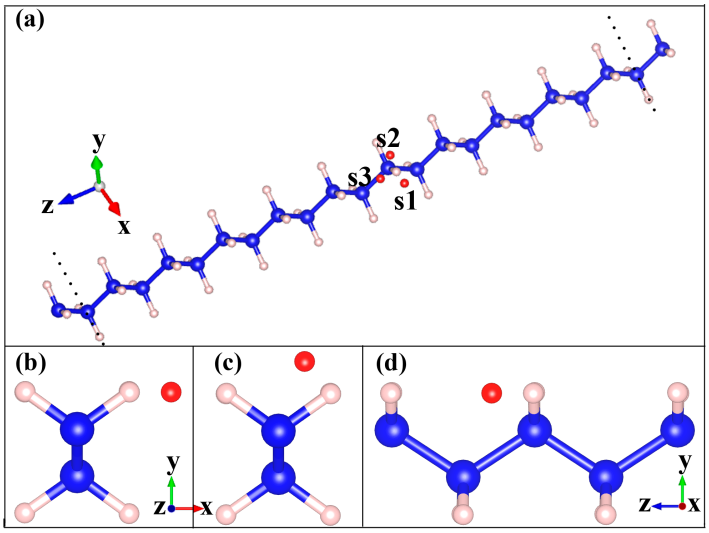

Figure 1. (Color online) (**a**) Stereogram of an infinitely long hydrocarbon chain with one H atom adsorbed at different sites. The two dotted lines show the borders of the supercell along the *z* direction. (**b**–**d**) are enlarged views of the adsorption sites of s1, s2, and s3, respectively. The blue, pink, and red balls denote the carbon, hydrogen, and the adsorbed H or H_2, respectively.

3. Results and Discussions

As shown in Table 1, the hydrogen atom had the lowest energy compared with the H_2 molecule case for all three adsorption sites considered. Thus, in the following, we will focus exclusively on the H adsorbed case. The most stable configuration was the hydrogen located at the site s1 with the adsorption energy of 1.19 eV. It was found that after the structural relaxation, all three initial adsorption sites transformed to the same final configuration. Namely, the adsorbed hydrogen cleaved one hydrogen atom from the hydrocarbon chain and a H_2 molecule was formed, fleeing away from the hydrocarbon chain. Thus, one dangling bond was left on the carbon atom in the chain, which caused the nearby carbon and hydrogen atoms in the chain to distort slightly. The adsorption energy of the final state was −0.15 eV. The negative value means the final state formed with H_2 was more stable than the initial state of the hydrocarbon chain and the isolated H atom. The bond lengths and bond angles of the carbon atoms with the dangling bonds in the chain varied substantially during the process. Compared to the intact case (1.52 Å), the bond length between the carbon atoms shrank about 0.05 Å, to 1.47 Å. The bond length between the carbon atom with the dangling bond and the left hydrogen atom also reduced slightly. These reductions of bond lengths can be ascribed to the enhanced charge density in the C-C and C-H bond area. In the process, the bond angle of C-C-C, in which the center atom is the carbon atom with the dangling bond, also changed from 113.6° to 120.8°, deviating much more from the regular tetrahedron angle (109.28°). The shortening of bond length and expansion of bond angle indicates that the characteristic of a C-C double bond had emerged.

Table 1. The adsorption energies of an infinitely long hydrocarbon chain with one H and H_2 adsorbed at s1, s2, and s3 sites in the supercell, respectively.

	E_a (eV)		
	s1	**s2**	**s3**
H	1.19	2.87	2.86
H_2	2.39	4.61	5.56

The ability of the incident H atom to cleave one hydrogen atom from the chain can be seen intuitively by the charge-density difference, calculated by the charge density of

a H atom adsorbed at site s1 minus the charge density of the pristine hydrocarbon chain (Figure 2a). For comparison, the charge density difference of the H_2 molecule adsorbed is given in Figure 2b. Figure 2a shows that the charge depletes in the C-H bond region, while in the H-H bond region, the charge accumulates. This charge transfer weakens the C-H bond and leads to the bond breaking eventually. While for the case of the H_2 molecule, the strong H-H bond in the H_2 molecule makes the splitting of the molecule hard. Therefore, Figure 2b shows that there is no obvious charge depletion in the C-H bond region. In Figure 2b, the left side of the charge distribution of the H_2 molecule changes slightly because of the attraction of the hydrogen atom in the hydrocarbon chain.

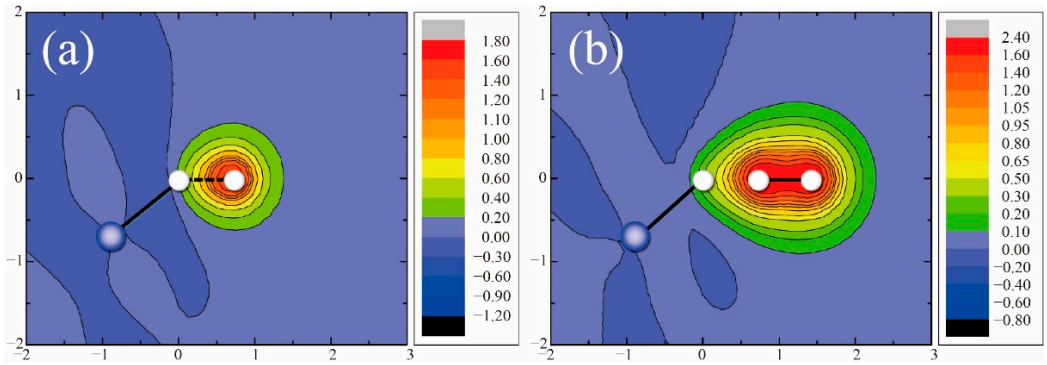

Figure 2. (Color online) The difference of the charge densities between the hydrocarbon chain with H (**a**) or H_2 (**b**) adsorbed at site s1 and the pristine hydrocarbon chain. The blue and white spheres are the carbon and hydrogen atoms, respectively.

Table 1 shows that the adsorption energies of the H adsorbed at all three sites are positive, indicating that the states of the H located at these sites were less stable than the state of the H far away from the chain. To understand the process clearly, the Nudged Elastic Band (NEB) method [38] was applied to investigate the energy profile for the whole reaction process of an incident H atom approaching the hydrocarbon chain and capturing a hydrogen atom, then forming a H_2 molecule and leaving the hydrocarbon chain. The incident H atom approaches the chain along the *x*-axis (Figure 3). It must pass over an energy barrier, about 1.4 eV, to reach the position where it can bond with the hydrogen atom in the hydrocarbon chain. Note, that even if the H_2 molecule reaches the bonding position, it cannot cleave the H atom from the chain, as indicated by the above analysis (Figure 2b). Therefore, the atomic hydrogen beam (AHB) [39,40] with a proper incident energy could be used as a hammer to knock off the hydrogen atom from the hydrocarbon chain, which offers better performance than H_2 molecule proposed by Trebicky et al. [27].

In the next step, we built a model of two infinitely long hydrocarbon chains in parallel along the *z*-direction to simulate the cross-linking effect. Each of the hydrocarbon chains had one hydrogen atom removed in the supercell, called R2 configuration. The initial and relaxed structures are shown in Figure 4a,b, respectively. After structural relaxation, the two carbon atoms with dangling bonds approached each other and form a C-C bond (Figure 4b). The bond length was 1.63 Å, comparable with the typical C-C single bond length (1.52 Å) in alkane chains. The positions of the adjacent carbon atoms and their bonded hydrogen atoms also deviated much from the ideal case, which made the cross-linking possible. The total energy difference for the configurations in Figure 4a,b was −89.87 eV ($E_{4(b)} - E_{4(a)}$), which shows that the cross-linking does help to stabilize the system. The charge-density difference is illustrated in Figure 4b, indicating that the electron accumulates in the cross-linking region, helping the formation of C-C direct bond. For comparison, we also calculated the two hydrocarbon chains, in which only one chain has a hydrogen atom removed (called the R1 configuration), and the two hydrocarbon chains with two hydrogen atoms per supercell removed from each chain individually (called R4). The calculations show that for the R1 case, no cross-linking was observed. Hence, the removal of at least one hydrogen atom per supercell from each chain (R2) was the minimum requirement

for the cross-linking between two hydrocarbon chains. While for the R4 configuration, the cross-linking happens, however, owing to the higher energy needed to cleave four hydrogen atoms totally per supercell, we suppose that this case is difficult to achieve in experiments, compared with the R2 configuration.

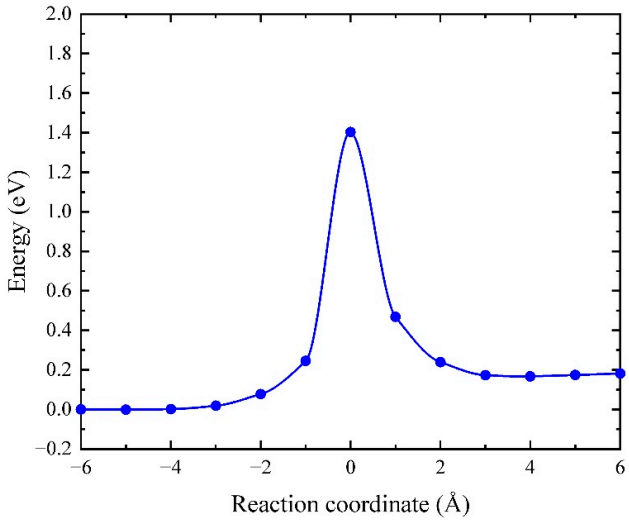

Figure 3. (Color online) The calculated minimum energy path (MEP). Blue circles correspond to NEB images. Reaction coordinate describes the process of an incident H atom approaching the hydrocarbon chain along the *x*-direction and fleeing away by detaching a hydrogen atom from the hydrocarbon chain and forming a H_2 molecule. Zero coordinate is set as the position of the H atom residing at the s1 position mentioned in Table 1.

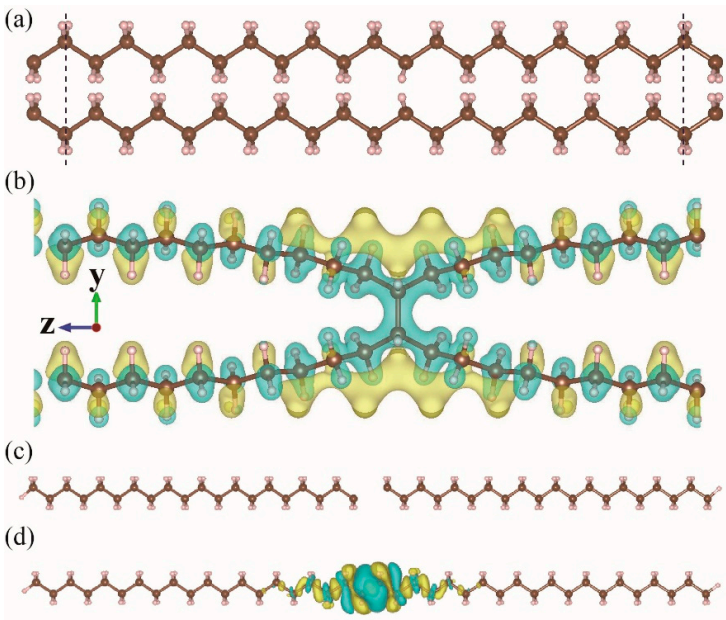

Figure 4. (Color online) The initial (**a**) and relaxed (**b**) structures of two infinitely long hydrocarbon chains in parallel along the *z*-axis. The two dotted lines in (**a**) show the borders of the supercell along the *z* direction. For each hydrocarbon chain, one hydrogen atom in the supercell is removed. Brown and pink spheres represent the carbon and hydrogen atoms, respectively. The charge-density difference is also given for the relaxed structure in (**b**). The green and yellow colors illustrate the electron accumulation and depletion regions, respectively. (**c**,**d**) are the initial and relaxed structures of two finitely long molecules ($C_{20}H_{42}$) in 'head-to-head' cross-linking mode. The charge-density difference for the relaxed structure is also given in (**d**). For each molecule, one hydrogen atom is removed.

To further understand the cross-linking, partial densities of states (DOSs) of the carbon atom with the dangling bond before and after the cross-linking are given in Figure 5 for the R2 configuration. In the initial state, the p_z hardly interacts with other three orbitals, while s, p_x, and p_y hybridize to each other and form sp^2 orbital. The unoccupied states above the Fermi level (E_F) indicate the existence of the dangling bonds. After structural optimization, the recombination of carbon orbitals makes the three p orbitals mix well with each other. The unoccupied states are pushed downward and filled.

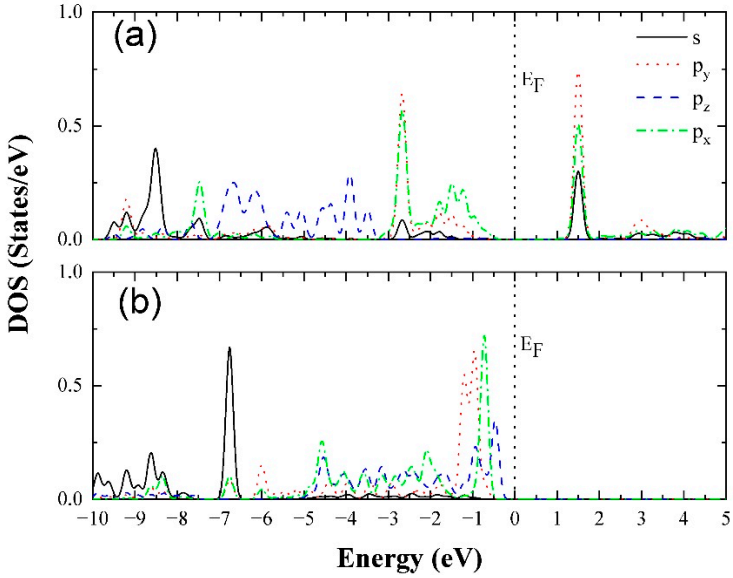

Figure 5. (Color online) The partial densities of states (DOSs) of the carbon atom with one of its connective hydrogens removed in the initial (**a**) and relaxed (**b**) structures for the R2 configuration.

Above, we considered the H dissociation and cross-linking of infinitely long hydrocarbon chains. Now, a finitely long alkane molecule, icosane ($C_{20}H_{42}$), is taken as an example, to observe what will happen in an experiment. The calculated binding energy shows that the incident H atom residing at the two ends of the $C_{20}H_{42}$ was more stable than at the position in the middle part of the molecule by 0.15 eV in energy. In the simulation of R2 configuration for $C_{20}H_{42}$ molecules, cross-linking also occurred as expected. Especially, the two $C_{20}H_{42}$ molecules can align 'shoulder-to-shoulder' (as shown in Figure 4a) or 'head-to-head' (seen Figure 4c). The energy of the 'head-to-head' alignment is found to be about 0.85 eV lower than the 'shoulder-to-shoulder' one because in the latter case, the neighboring H atoms of the two molecules repel each other, resulting in the system unstable relatively.

In the 'head-to-head' mode, the cross-linking caused the two $C_{20}H_{42}$ molecules to connect and form a longer molecule $C_{40}H_{82}$, as illustrated in Figure 4d. We could see from it that the charge also accumulated in the bond region. Vries et al. found that by bombarding frozen methane molecules, much longer hydrocarbon molecules containing at least 13 atoms were detected [41]. While Moore et al. investigated ion-irradiated water-ice mixtures and found C_2H_6 could be yielded by CH_4 dimerization [42]. Our calculations indicate that hydrogen bombardment can also lead to the polymerization, thus benefit the formation of long chain hydrocarbon molecules. These results are important to understand the synthesis mechanism of complex organic molecules from quite simple hydrocarbon molecules in organic chemistry and astrophysics.

The 'shoulder-to-shoulder' cross-linking may also happen when the dangling bonds are in the middle of $C_{20}H_{42}$ molecules instead of at the two ends of the molecules. Although the dangling bond is easier to form at the ends of the molecules, the incident H atom may have a large probability to hit the H atom located in the middle part of the target molecules, especially for long molecules. Thus, for longer hydrocarbon molecules, 'shoulder-to-shoulder' cross-linking may occur more easily. In experimental work dis-

played for Dotriacontane $C_{32}H_{66}$, the 'shoulder-to-shoulder' cross-linking made the thin film form perpendicular to the substrate and enhanced the mechanical properties of the film [12]. For shorter molecules, longer molecules can be fabricated through the 'head-to-head' cross-linking mode. However, we must emphasis the preference of the cross-linking mode highly depends on the experimental conditions, such as the arrangement of the molecules. Further investigation should be made to explore the abundant phenomena of cross-linking in alkane molecules with different lengths. In addition, we should mention that besides the hydrocarbon molecules with a chain structure, our conclusion may also apply to the cross-linking of hydrocarbon molecules with a ring-like structure, such as aromatic molecules, or complex hydrocarbon molecules with extra functional groups.

4. Conclusions

In summary, calculations of the structural and electronic properties of H incidence induced hydrogen dissociation and cross-linking of hydrocarbon chains of self-assembled monolayers were performed. At the three initial adsorption sites, the incident H can detach one hydrogen atom from the hydrocarbon chains to form a H_2 molecule and flee away. Among H atoms and H_2 molecules, H atoms may be the better candidate to cleave the hydrogen atoms from the chains. The 'head-to-head' cross-linking was found to be more energetically favorable than the 'shoulder-to-shoulder' mode. It is expected that in experiments, the long molecules may prefer the 'shoulder-to-shoulder' cross-linking, while short molecules may prefer the cross-linking mode of 'head-to-head'. Our results show that hyperthermal hydrogen can be a very efficient tool to produce large hydrocarbon chains or even ultrathin organic films. Our study should be helpful for the enhancement of mechanical and chemical strength of self-assembled monolayers and enlarge the scope of the application of low-dimensional organic materials.

Author Contributions: Methodology, Y.Z.; software, X.-Y.W.; validation, Y.Z. and X.-Y.W.; formal analysis, R.X.; data curation, Y.Z. and R.X.; writing—original draft preparation, Y.Z.; writing—review and editing, R.X. All authors have read and agreed to the published version of the manuscript.

Funding: This research was funded by the National Natural Science Foundation of China, grant No. 21104028, and the Natural Science Foundation of Shanghai, grant No. 14ZR1403400. All theoretical calculations were performed at the High Performance Computational Center (HPCC) of Department of Physics, Fudan University.

Data Availability Statement: Not applicable.

Acknowledgments: Xinyuan Wei thanks the China Scholarship Council (CSC) for financial support. Yan Zhu thanks the 2014 Competitive Grant Program of Overseas Returnees Research Projects for financial support.

Conflicts of Interest: The authors declare no conflict of interest.

References

1. Joseph, S.; Varandas, A.J.C. Ab initio Based DMBE Potential Energy Surface for the Ground Electronic State of the C_2H Molecule. *J. Phys. Chem. A* **2010**, *114*, 2655–2664. [CrossRef] [PubMed]
2. Daugulis, O.; Roane, J.; Tran, L.D. Bidentate, Monoanionic Auxiliary-Directed Functionalization of Carbon−Hydrogen Bonds. *Acc. Chem. Res.* **2015**, *48*, 1053–1064. [CrossRef] [PubMed]
3. Azizollahi, H.; García-López, J.-A. Recent Advances on Synthetic Methodology Merging C–H Functionalization and C–C Cleavage. *Molecules* **2020**, *25*, 5900. [CrossRef] [PubMed]
4. Fazekas, T.J.; Alty, J.W.; Neidhart, E.K.; Miller, A.S.; Leibfarth, F.A.; Alexanian, E.J. Diversification of aliphatic C–H bonds in small molecules and polyolefins through radical chain transfer. *Science* **2022**, *375*, 545–550. [CrossRef]
5. Lazar, P.; Schollmeyer, H.; Riegler, H. Spreading and Two-Dimensional Mobility of Long-Chain Alkanes at Solid/Gas Interfaces. *Phys. Rev. Lett.* **2005**, *94*, 116101. [CrossRef]
6. Knüfing, L.; Schollmeyer, H.; Riegler, H.; Mecke, K. Fractal analysis methods for solid alkane monolayer domains at SiO_2/air interfaces. *Langmuir* **2005**, *21*, 992–1000. [CrossRef]
7. Yamamoto, T.; Nozaki, K.; Yamaguchi, A.; Urakami, N. Molecular simulation of crystallization in n-alkane ultrathin films: Effects of film thickness and substrate attraction. *J. Chem. Phys.* **2007**, *127*, 154704. [CrossRef]

8. Nie, H.Y. Self-assembled monolayers of octadecylphosphonic acid and polymer films: Surface chemistry and chemical structures studied by time-of-flight secondary ion mass spectrometry. *Surf. Interface Anal.* **2017**, *49*, 1431–1441. [CrossRef]
9. Woon-Ming, L. From surface science research to high-impact knowhows Exemplars of Surface Science Western. *Surf. Interface Anal.* **2017**, *49*, 1292–1297.
10. Nie, H.Y. Negative hydrocarbon species $C_{2n}H^-$: How useful can they be? *J. Vac. Sci. Technol. B* **2016**, *34*, 030603. [CrossRef]
11. Du, W.L.; Shao, H.; He, Z.K.; Tang, C.Y.; Liu, Y.; Shen, T.; Zhu, Y.; Lau, W.M.; Hui, D. Cross-Linking Poly(lactic acid) Film Surface by Neutral Hyperthermal Hydrogen Molecule Bombardment. *J. Agric. Food Chem.* **2015**, *63*, 10604–10610. [CrossRef]
12. Liu, Y.; Yang, D.Q.; Nie, H.Y.; Lau, W.M.; Yang, J. Study of a hydrogen-bombardment process for molecular cross-linking within thin films. *J. Chem. Phys.* **2011**, *134*, 074704. [CrossRef] [PubMed]
13. Patten, T.E.; Xia, J.H.; Abernathy, T.; Matyjaszewski, K. Polymers with Very Low Polydispersities from Atom Transfer Radical Polymerization. *Science* **1996**, *272*, 866–868. [CrossRef] [PubMed]
14. Lutz, J.F.; Schmidt, B.V.K.J.; Pfeifer, S. Tailored polymer microstructures prepared by atom transfer radical copolymerization of styrene and N-substituted maleimides. *Macromol. Rapid Commun.* **2011**, *32*, 127–135. [CrossRef] [PubMed]
15. Zorvaryan, A.; Inceoglu, S.; Acar, M. Alkylation of polyethyleneimine for homogeneous ligands in ATRP. *Polymer* **2011**, *52*, 617–621. [CrossRef]
16. Santonicola, M.G.; Groot, G.W.; Memesa, M.; Meszyńska, A.; Vancso, G.J. Reversible pH-controlled switching of poly (methacrylic acid) grafts for functional biointerfaces. *Langmuir* **2010**, *26*, 17513–17519. [CrossRef]
17. Fabio, d.L.; Matyjaszewski, K. Transition metal catalysts for controlled radical polymerization. *Prog. Polym. Sci.* **2010**, *35*, 959–1021.
18. Andersen, C.A.; Roden, H.J.; Robinson, C.F. Negative Ion Bombardment of Insulators to Alleviate Surface Charge-Up. *J. Appl. Phys.* **1969**, *40*, 3419–3420. [CrossRef]
19. Zhu, Z.; Stevie, F.A.; Griffis, D.P. Model study of electron beam charge compensation for positive secondary ion mass spectrometry using a positive primary ion beam. *Appl. Surf. Sci.* **2008**, *254*, 2708–2711. [CrossRef]
20. Arnold, J.C.; Sawin, H.H. Charging of pattern features during plasma etching. *J. Appl. Phys.* **1991**, *70*, 5314–5317. [CrossRef]
21. Bao, J.; Shi, H.; Huang, H.; Ho, P.S. Oxygen plasma damage to blanket and patterned ultralow-κ surfaces. *J. Vac. Sci. Technol.* **2010**, *28*, 207–215. [CrossRef]
22. Despiau-Pujo, E.; Chabert, P. Velocity distribution function of sputtered gallium atoms during inductively coupled argon plasma treatment of a GaAs surface. *J. Vac. Sci. Technol. A* **2010**, *28*, 356–361. [CrossRef]
23. Vozniy, O.V.; Yeom, G.Y. High-energy negative ion beam obtained from pulsed inductively coupled plasma for charge-free etching process. *Appl. Phys. Lett.* **2009**, *94*, 231502. [CrossRef]
24. Zheng, Z.; Xu, X.D.; Fan, X.L.; Lau, W.M.; Kwok, R.W.M. Ultrathin polymer film formation by collision-induced cross-linking of adsorbed organic molecules with hyperthermal protons. *J. Am. Chem. Soc.* **2004**, *126*, 12336–12342. [CrossRef] [PubMed]
25. Zheng, Z.; Kwok, W.M.; Lau, W.M. A new cross-linking route via the unusual collision kinematics of hyperthermal protons in unsaturated hydrocarbons: The case of poly(trans-isoprene). *Chem. Commun.* **2006**, *29*, 3122–3124. [CrossRef]
26. Zheng, Z.; Wong, K.W.; Lau, W.C.; Kwok, R.W.M.; Lau, W.M. Unusual kinematics-driven chemistry: Cleaving C–H but not COO–H bonds with hyperthermal protons to synthesize tailor-made molecular films. *Chem. Eur. J.* **2007**, *13*, 3187–3192. [CrossRef]
27. Trebicky, T.; Crewdson, P.; Paliy, M.; Bello, I.; Nie, H.Y.; Zheng, Z.; Fan, X.L.; Yang, J.; Gillies, E.R.; Tang, C.Y.; et al. Cleaving C–H bonds with hyperthermal H_2: Facile chemistry to cross-link organic molecules under low chemical- and energy-loads. *Green Chem.* **2014**, *16*, 1316–1325. [CrossRef]
28. Jacobs, D.C. Reactive Collisions of Hyperthermal Energy Molecular Ions with Solid Surfaces. *Annu. Rev. Phys. Chem.* **2002**, *53*, 379–407. [CrossRef]
29. Ocko, B.M.; Wu, X.Z.; Sirota, E.B.; Sinha, S.K.; Gang, O.; Deutsch., M. Surface freezing in chain molecules: Normal alkanes. *Phys. Rev. E* **1997**, *55*, 3164. [CrossRef]
30. Abdallah, D.J.; Weiss, R.G. n-Alkanes Gel n-alkanes (and many other organic liquids). *Langmuir* **2000**, *16*, 352–355. [CrossRef]
31. Blöchl, P.E. Projector augmented-wave method. *Phys. Rev. B* **1994**, *50*, 17953–17979. [CrossRef] [PubMed]
32. Kresse, G.; Joubert, D. From ultrasoft pseudopotentials to the projector augmented-wave method. *Phys. Rev. B* **1999**, *59*, 1758–1775. [CrossRef]
33. Kresse, G.; Hafner, J. Norm-conserving and ultrasoft pseudopotentials for first-row and transition elements. *J. Phys. Condens. Matter* **1994**, *6*, 8245–8257. [CrossRef]
34. Perdew, J.P.; Wang, Y. Accurate and simple analytic representation of the electron-gas correlation energy. *Phys. Rev. B* **1992**, *45*, 13244–13249. [CrossRef]
35. Kresse, G.; Furthmüller, J. Efficiency of Ab-Initio Total Energy Calculations for Metals and Semiconductors Using a Plane-Wave Basis Set. *Comput. Mater. Sci.* **1996**, *6*, 15–50. [CrossRef]
36. Monkhorst, H.J.; Pack, J.D. Special Points for Brillouin-Zone Integrations. *Phys. Rev. B* **1976**, *13*, 5188–5192. [CrossRef]
37. Momma, K.; Izumi, F. VESTA 3 for Three-Dimensional Visualization of Crystal, Volumetric and Morphology Data. *J. Appl. Crystallogr.* **2011**, *44*, 1272–1276. [CrossRef]
38. Mills, G.; Jonsson, H.; Schenter, G.K. Reversible work transition state theory: Application to dissociative adsorption of hydrogen. *Surf. Sci.* **1995**, *324*, 305. [CrossRef]

39. Van, Z.B.; Utterback, N.G.; Amme, R.C. Charged-particle production in low-energy $H+H_2$ and $H+H_e$ collisions. *Rev. Sci. Instrum.* **1976**, *47*, 314–323.
40. Hughes, P.P.; Coplan, M.A.; DeFazio, J.N.; Chornay, D.J.; Collier, M.R.; Ogilvie, K.W.; Shappirio, M.D. Scattering of neutral hydrogen at energies less than 1 keV from tungsten and diamondlike carbon surfaces. *J. Vac. Sci. Technol. A* **2009**, *27*, 1188–1195. [CrossRef]
41. de Vries, A.E.; Pedrys, R.; Haring, R.A.; Haring, A.; Saris, F.W. Emission of large hydrocarbons from frozen CH_4 by keV proton irradiation. *Nature* **1984**, *311*, 39–40. [CrossRef]
42. Moore, M.H.; Hudson, R.L. Infrared Study of Ion-Irradiated Water-Ice Mixtures with Hydrocarbons Relevant to Comets. *Icarus* **1998**, *135*, 518–527. [CrossRef]